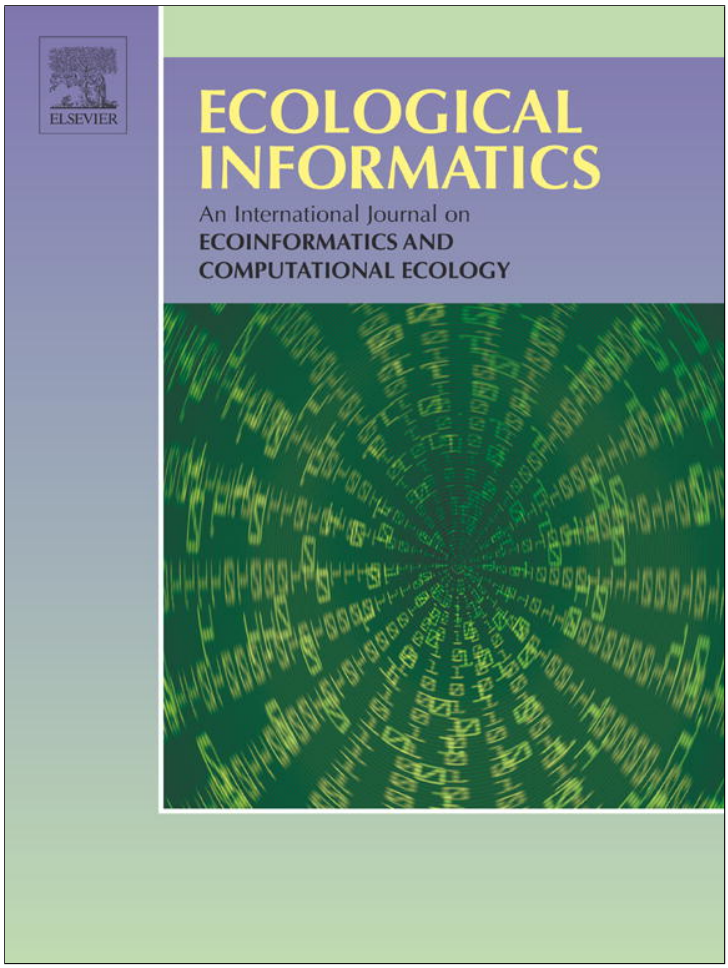

(This is a sample cover image for this issue. The actual cover is not yet available at this time.)

Ecological Informatics 13 (2013) 57–69

Contents lists available at SciVerse ScienceDirect

Ecological Informatics

journal homepage: www.elsevier.com/locate/ecolinf

Modelling competitive ability of Neotropical savanna grasses: Simulation of shading and drought impacts on biomass production

J. Segarra [a,*], J. Raventós [a], M.F. Acevedo [b,c], J.F. Silva [d], C. Garcia-Núñez [d]

[a] Departamento de Ecología, Universidad de Alicante, Alicante, Spain
[b] Electrical Engineering Department, Geography Department, and Environmental Science Program, University of North Texas, Denton, TX 76203, USA
[c] Center for Simulation and Modeling (CESIMO), Universidad de los Andes, Mérida, Venezuela
[d] Instituto de Ciencias Ambientales y Ecológicas (ICAE), Universidad de los Andes, Mérida, Venezuela

ARTICLE INFO

Article history:
Received 16 February 2012
Received in revised form 2 October 2012
Accepted 10 October 2012
Available online 17 October 2012

Keywords:
Biomass
Drought
Grasses
Convolution
Transition matrix
Evapotranspiration

ABSTRACT

In this paper, we develop a technique to model the spatial distribution of shoots along vertical and horizontal dimensions of a plant community. We use it to simulate the growth of a tropical savanna near the city of Barinas, Venezuela, to explore the responses of the peak biomass of a plant community to a range of 10-50% reduction of rainfall. We selected three dominant grass species: *Elyonurus adustus*, *Leptocoryphium lanatum*, and *Andropogon semiberbis* in a 4×7 m study plot. We estimate parameters values from data measured in the field. The number of shoots for each plant is obtained according to soil water availability and distributed vertically by 10 cm levels using a transition matrix. Convolution allows calculation of leaf area index for each cell and vertical level, which is then used to calculate light attenuation and thus the proportion of shaded shoots in each cell and level. With this information, maximum evapotranspiration is determined to calculate soil moisture using daily rain time series. Biomass is calculated for all species based on shoot biomass measured in the field and fire is simulated by removing a fraction of the shoots segments of all species. Modeled biomass fits reasonably well to field data.

The model predicts significant differences in the response of each species to drought. *A. semiberbis* was the most drought resistant of the three species, whereas *L. lanatum* was the least, and *E. adustus* was intermediate, in agreement with observations in the literature. Our model suggests that drought resistance increases with the biomass/transpiration ratio for the species considered.

1. Introduction

The savanna is one of the most important biomes of the planet covering at least 20% of the global land surface and in some cases acts as a transition between tropical rainforest and deserts (Sarmiento, 1983). Savannas are found in a wide gradient of physiognomies from woodland to grassland and they have high environmental and economic value (Solbrig, 1993). Due to its ecological importance, the tropical savanna has been widely modeled to simulate one or several of four principal determinants of its structure: soil moisture, soil nutrients, herbivory, and fire (see reviews of Hill and Hanan, 2010; Sankaran et al., 2004; Staver et al., 2011a,b).

Climate models predict diminishing trends of rainfall for the region containing the study area (Dai, 2010; Mata, 1996). For this reason, we have developed a model to study the response to drought of some types of dominant grasses in the savanna, based on Segarra et al. (2009). In that paper we presented a theoretical stochastic model of root competition for water, which couples soil water availability, phenology, and root and shoot architecture applied to three Neotropical savanna grasses. Competition among neighboring plants took into account soil moisture and the spatial distribution of the individuals. The model determines the water requirements of each plant (in function of their biomass and its rate of transpiration), and then calculated, using the convolution technique, how the demand for water is distributed among the surrounding space. Using these data, we compared the behavior of isolated plants, pairs and trios, and we found belowground competition to be a fundamental component of global (shoot + root) competition. (See Appendix A for more details).

In this paper, we propose an extension of Segarra et al. (2009) model to determine the shading from neighboring plants. Recent ecological models tend to separate the canopy leaves into sunlit and shaded categories, which is found to provide a considerable advantage and improvement in the scale-up calculations of photosynthesis and transpiration from leaf to canopy (Gates, 2003; Wang et al., 2001). In particular, shading is important to model the effect of drought on transpiration and photosynthesis (Aranda et al., 2005; Ashton et al., 2006).

Models of light interception by the canopy fall into two categories. First, precise models, taking into account the exact position of every

* Corresponding author at: Universidad de Alicante. Campus de Sant Vicent del Raspeig. Ap. 99 E-03080 (Alicante), Spain.
E-mail address: josegsegarra@yahoo.es (J. Segarra).

1574-9541/$ – see front matter © 2012 Elsevier B.V. All rights reserved.
http://dx.doi.org/10.1016/j.ecoinf.2012.10.003

leaf, angle of incidence and the angle of leaves (de Moraes Frasson and Krajewski, 2010; Sekimura et al., 2000). All these models showed good agreement with field data but are not adequate for large plots with many individual plants or for simulations at a daily time scale, since computing time would be too long.

Second, models that calculate incoming radiation from the canopy surface without considering shoot angle (Thornley, 2002), or those that focus on above and below ground competition using convolution techniques (Barbier et al., 2008). These models execute faster than the models that include geometric details but do not account for plant morphology.

Our paper is in between these two approaches; it uses fast computing convolution techniques (which we explain in Appendix A) and incorporates architectural traits of the plants. Consequently, the model allows working with large plant communities in a precise and rapid manner, using calculations for whole populations. Moreover, the calculation of the spatial structure of each plant is easier than with other models because it does not need to know the spatial position of each shoot, but the entire set of shoots of each level is calculated statistically.

In this paper, we model the dynamics of plant growth at two different levels: a) plant level, taking into account vertical structure; b) community level, taking into account interspecific interactions among several plants. In order to simulate the drought scenarios the model calculates the transpiration rates taking into account the spatial arrangement of the shoots, because transpiration rates could be higher in sun-exposed leaves compared with shaded ones. Further, we apply this technique at each vertical level each 10 cm in height in order to take into account shading of shoots. Here we call 'shoot' the aerial part of the plant which includes stem, sheath and leaf. Besides, the model also takes into account the effect of fire, therefore including two of the most crucial factors in the structure of the savanna: fire and soil moisture (Accatino et al., 2010).

Our specific objectives are: 1) model shoot shading and transpiration rates, by adding spatial distribution of shoots along the vertical direction to our previous competition model (Segarra et al., 2009); 2) explore the effects of drought scenarios on biomass, and develop a metric of plant resistance to drought.

2. Study site and field methods

The study site corresponds to a seasonal savanna near the city of Barinas, Venezuela (8° 38′ N, 70° 12′ W). Mean annual temperature is 27 °C and mean annual rainfall is 1250 mm, with a rainy season from May to November and a dry season from January to March. We selected three grass species with different phenologies and architectures, common in Neotropical savannas: 1) *Elyonurus adustus*, (Trin.) E. Ekman, a precocious growing, bunch grass with long and slender leaves; 2) *Leptocoryphium lanatum*, (Kunth) Nees, an early growing, bunch grass with long coriaceous and narrow leaves; and 3) *Andropogon semiberbis*, (Nees) Kunth, a tall and late flowering bunch grass, with short herbaceous leaves. For brevity, these three species will be denoted by the codes *E*, *L*, and *A* respectively.

A first set of field data comes from a detailed sampling conducted at this site by Raventós and Silva (1988). Three individual plants (replicates) of each species were measured using a structure in which a horizontal frame of 225 (15×15) cells of 5×5 cm was set at different heights. For one year, monthly measurements of module density by height were performed from 10 to 140 cm above ground at 10 cm intervals (vertical levels). The maximum number of levels achieved by a plant during the year varies by replicate and species; typically five levels for *E*, seven for *L*, and ten for *A*. For more details see Acevedo and Raventós (2002) and Raventós et al. (2004). A second set of data was obtained in April 2006 from sampling a rectangular area of 4×7 m at this site, measuring the coordinates of each individual plant and the number of shoots. The soil texture is loamy sand.

We also measured transpiration, stomatal conductance, and CO_2 assimilation of the three species at different times of day and in two periods: in April 2006 (rainy season) and February 2007 (wet season).

We used daily precipitation data from the weather station 804400 (SVBI) in the State of Barinas, Venezuela, (8° 61′ N, 70° 21′ W, altitude 202 m) for the period 1991–2007 (TuTiempo.com, 2011). These data were checked for homogeneity (Alexandersson, 1986) and their monthly averages are summarized in Table 1.

3. Spatial resolution, time scales, and model steps

The model spatial domain is the 4×7 m plot which is divided in two nested horizontal grids. One grid is low-resolution of 1×1 m squares for soil moisture calculation, hereafter referred as 'quadrats', and the other is high-resolution with squares of 1×1 cm for shoot number calculation, hereafter referred to as 'cells'. Thus, there are 100×100 cells in a quadrat. The low- resolution grid defines matrices of dimension 4×7, with rows and columns denoted by (*ix*,*iy*), whereas the high-resolution grid defines matrices of dimension 400×700, with rows and columns denoted by (*kx*,*ky*). Aboveground, up to 140 cm, the spatial domain is divided in vertical levels of 10 cm, whereas belowground is vertically homogeneous.

For each quadrat, soil moisture dynamics is calculated daily using simulated rain time series and shoot distribution. Conversely, plant growth and shoot distribution is calculated on a monthly basis using monthly averages of soil moisture.

Fig. 1 summarizes the model whose steps are briefly described below. In the following sections we give the details for each calculation.

- Step 1) Number of shoots for each plant at basal vertical level is obtained monthly according to the monthly average of soil water availability in the corresponding quadrat and species specific parameters.
- Step 2) From the number of shoots at the basal vertical level we determine the number of shoot segments at each higher level using a transition matrix. A shoot segment is the portion of a shoot between two consecutive vertical levels.
- Step 3) Using the high-resolution horizontal grid, we horizontally spread the shoot number of each level by calculating the convolution of a species-specific kernel with the shoot number for all plants at that vertical level. These data are used to build a 400×700 matrix for each species with entries equal to the number of shoot segments for each cell and vertical level.
- Step 4) Leaf area index (LAI) is calculated for each cell and level. This calculation is made using the matrices of shoot segments calculated above.
- Step 5) LAI values are used to calculate the proportion of light transmitted for each cell and level. We assume that this proportion is 1 at the top level where all shoot segments receive direct radiation. For each species, using the proportion of shoot segments receiving direct radiation at each level we build a matrix with entries giving the proportion of shade in each cell and level.
- Step 6) Multiplying the proportion of shade by the number of shoots segments in each cell we obtain the number of shoot segments under shade and under direct radiation for each species.
- Step 7) Maximum evapotranspiration, by species and total, is then calculated at each cell and aggregated to the quadrat to obtain a value for the month at each quadrat.
- Step 8) Holding maximum evapotranspiration constant for every day of the month, soil moisture is calculated in each quadrat on a daily basis, using te simulated daily rain time series. We then use monthly averages of soil moisture in each quadrat to calculate shoot production and mortality for each plant in the quadrat, going back to step 1.

Table 1
Monthly rainfall for Barinas, Venezuela. The first three rows are obtained from the 1991–2007 dataset of station 804400 (SVBI). H_m: mean monthly precipitation; H_{sd}: standard deviation; J_m: average number of rain days per month.

	Jan	Feb	Mar	Apr	May	Jun	Jul	Aug	Sep	Oct	Nov	Dec
H_m(mm)	13.1	9.4	34.1	64.1	151.5	184.6	164.1	209.9	190.8	124.7	83.5	20.5
H_{sd}(mm)	27.3	18.5	31.2	50.6	92.8	100.6	79.3	101.2	122.9	58.7	50.6	39.4
J_m	4	5	6	7	10	11	12	14	15	12	12	9

Step 9) Biomass is calculated in each cell for all species and aggregated to the quadrat. This step is performed after step 3 as a side calculation and does not form part of the simulation loop.
Step 10) Each February the model kills 90% of the shoots segments of all species in order to simulate mortality by fire.

3.1. Step 1: number of shoots

The total number of shoots of plant k of species j is the number at base level or vertical level 1, which we denote as $n^1_{j,k}(t)$. This number is given by a balance of gross production and mortality modeled by Richard's equation (Segarra et al., 2005, 2009) calculated on a monthly basis

$$\frac{dn^1_{j,k}(t)}{dt} = \frac{b_j\left(\bar{s}_{ix,iy}(t)\right) - \mu_j\left(\bar{s}_{ix,iy}(t)\right)}{g_j} n^1_{j,k}(t)\left(1 - \left(\frac{n^1_{j,k}(t)}{N_j}\right)^{g_j}\right) \quad (1)$$

where: g_j is a coefficient controlling the shape of the function (dimensionless), N_j is maximum number of shoots, $b_j\left(\bar{s}_{ix,iy}(t)\right)$ is the gross shoot production rate (month^{-1}), and $\mu_j\left(\bar{s}_{ix,iy}(t)\right)$ is shoot mortality rate (month^{-1}). Both rates are dependent on soil water availability $\bar{s}_{ix,iy}(t)$ (monthly average) at the quadrat of row ix, column iy where plant k is located. Functions $b_j\left(\bar{s}_{ix,iy}(t)\right)$ and $\mu_j\left(\bar{s}_{ix,iy}(t)\right)$ use parameters $b_{j\max}$ and $\mu_{j\max}$ respectively. These functions and soil moisture calculation are explained in a later section. Parameter values are given in Table 2.

Initial conditions for shoot number $n^1_{j,k}(0)$ were assigned from the values obtained from sampling the rectangular 4×7 m plot at the site specified in paragraph 2, giving the location coordinates of each individual plant and its number of shoots as described in the previous section. These data were measured in April therefore the model starts calculations in that month. For soil water, initial conditions $\bar{s}_{ix,iy}(0)$ were assigned the value 0.2 for all quadrats, which is April's soil moisture according to Segarra et al. (2009).

3.2. Step 2: shoots segments by level

In Segarra et al. (2009) we calculated number of shoots as a function of available soil water only and ignored growth restrictions due to shading. To model effects of shading we need to know the spatial distribution of shoots segments at each level. For this we use the matrix model from Raventós et al. (2004) structured by 10 cm vertical levels. The three species differ in the maximum height reached by the end of the growing season: *A* reaches 10 levels, *L* reaches 7 levels and *E* reaches 5 levels.

Let's denote $\mathbf{n}_{j,k}(t)$ as the vector of number of shoot segments for plant k of species j, at time t, with entries $n^i_{j,k}(t)$ given by number of segments at level i. As explained in the previous section, the total number of shoots of plant k is the number at base level or level 1, $n^1_{j,k}(t)$. A matrix equation is applied monthly to all plants of each of the three species j in order to distribute the number of shoots of each plant by level

$$\mathbf{n}_{j,k}(t+1) = \mathbf{M}_j\left(\mathbf{n}_{j,k}(t) \circ \boldsymbol{\rho}_{j,k}(t+1)\right) \quad (2)$$

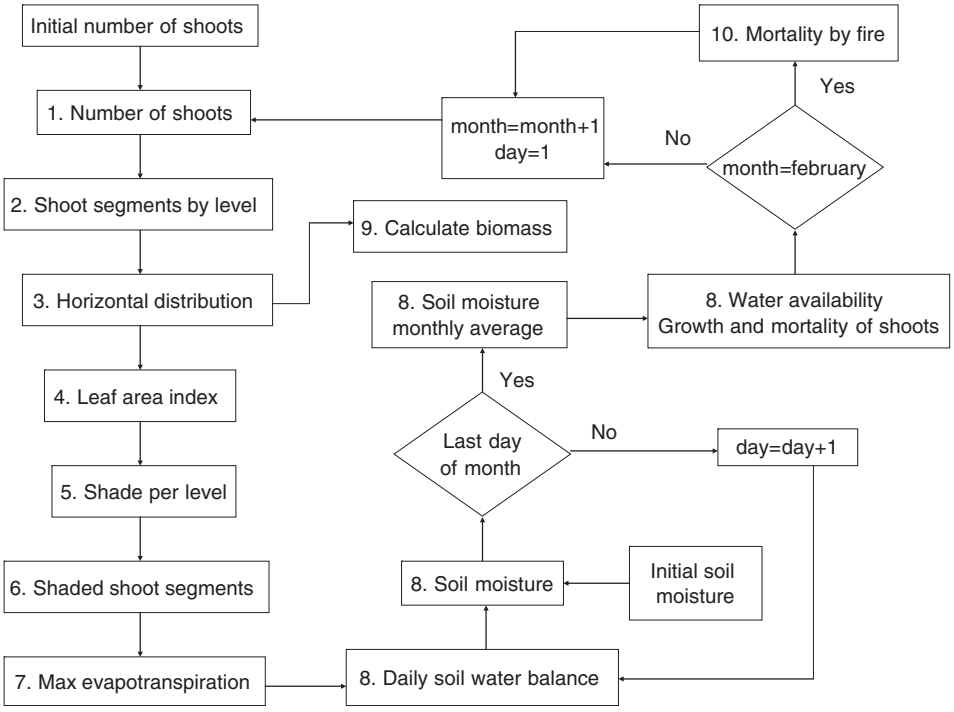

Fig. 1. Calculation steps followed in the model.

Table 2
Parameter values used to calculate shoot growth (from Segarra et al., 2009) and parameters used to estimate dispersion coefficient $D_{j,i}$ of bidimensional kernel.

Species	Shoot growth				Dispersion kernel		
	g_j	b_{jmax}	μ_{jmax}	N_j	c_j	d_j	f_j
E	0.2	0.6	1	850	1.872	−0.971	0.146
L	0.2	0.6	1	360	1.066	0.594	0.342
A	0.2	1	1	110	1.965	−0.992	0.097

where $\mathbf{M}_j$ is a square level-transition matrix for species *j* with entries representing the transition from one level to levels above, $\boldsymbol{\rho}_{j,k}(t+1)$ is a ratio of shoot number change due to emergence and mortality described later, and the symbol ◦ represents the Hadamard or entry-wise product of the two vectors. For more details see Appendix B.

3.3. Step 3: horizontal distribution of shoot segments

To determine the horizontal spatial distribution, along axes *x* and *y*, of shoot segments of all species at each level we use the convolution technique and a species-specific distribution kernel.

To obtain the horizontal distribution $S_{j,i}(x,y,t)$ of shoot segments of all plants of species *j* at each level *i* at time *t* we calculate the convolution between $V_{j,i}(x,y,t)$ (a matrix indicating the number of shoots that there are in the position x,y) and the kernel $K_{j,i}(x,y)$.

The kernel is shown in Fig. 2, where we compared the densities of shoot segments calculated from the kernel $K_{j,i}(x,y)$ to those from field data for each species using two levels, the first (lowest) and a second one corresponding to the mid-height of the plant. Agreement between the field data and the kernel results is better for *E* and *L* than *A*, and also better at level 1 than at the middle level. This indicates

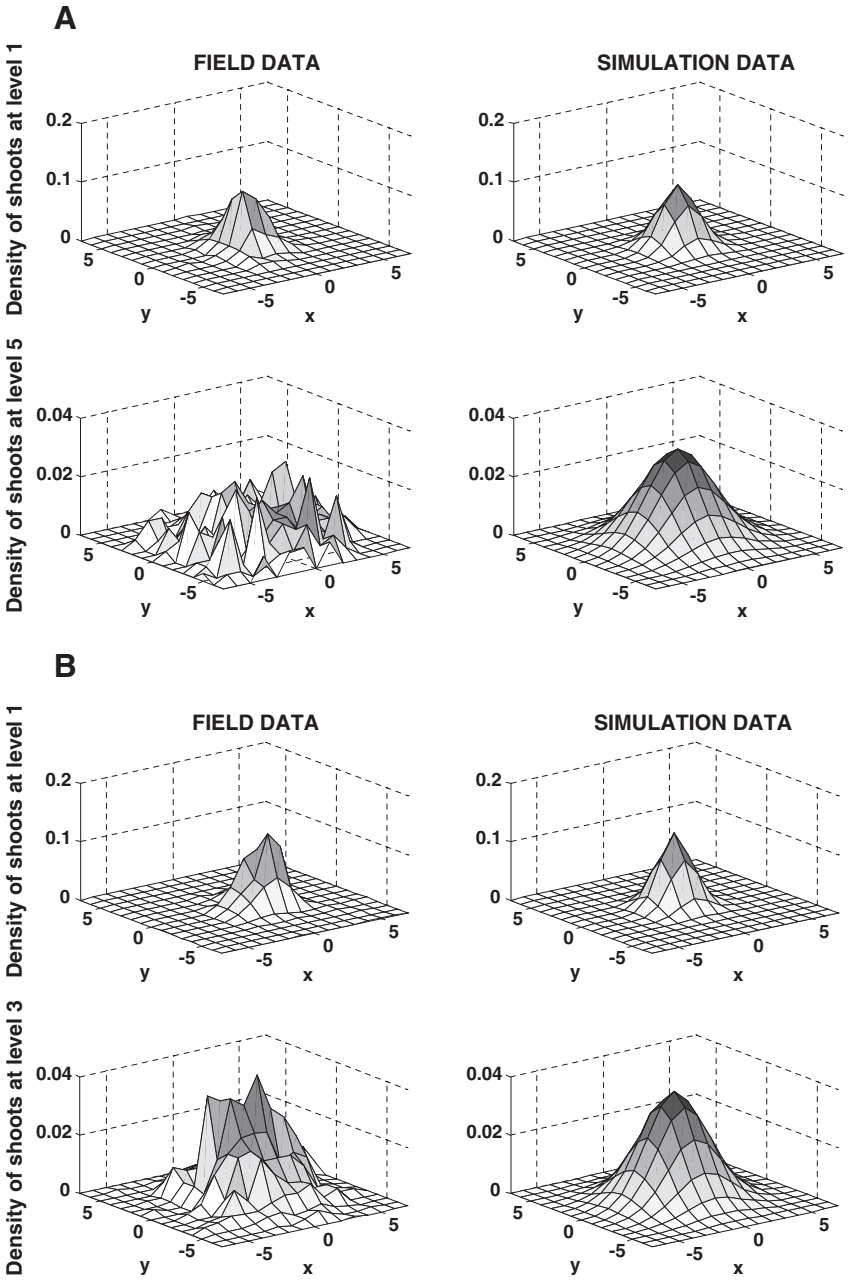

Fig. 2. Spatial distribution of the frequency of shoot segments in 25 cm^2 cells for each of the species. A) *Andropogon semiberbis*, B) *Elyonurus adustus*, and C) *Leptocoryphium lanatum*. Two vertical levels are plotted: level 1 and the level corresponding to the species' average height. These distributions are used to obtain the distribution kernel of shoot segments. The coordinates x and y are spatial coordinates, with the origin (0.0) centered on the central axis of the plant.

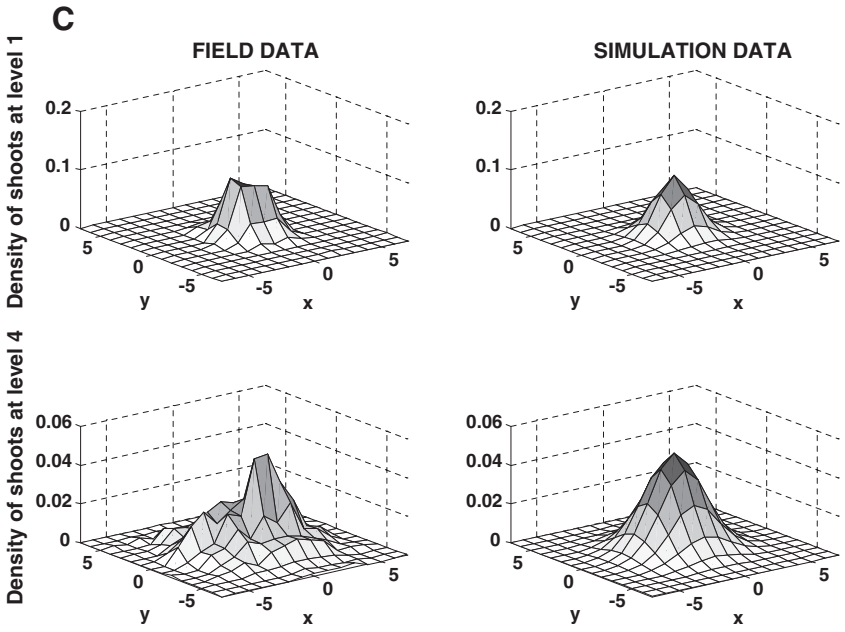

Fig. 2 (*continued*).

that agreement is better for those species with higher number of shoots (*E* and *L*) and also when segments are less dispersed, as is the case at level 1.

Adjustment between shoot segments distributions from the kernel model and those from field data are very acceptable as suggested by the mean quadratic errors shown in Table 3. For this comparison we calculated the kernel using a 5×5 cm cell size since these are the dimensions of the field sampling cells (Fig. 2). Later, for simulations we interpolated to another kernel of the same shape but calculated at the high-resolution cells of 1×1 cm.

Fig. 3 shows the coordinates of each plant position in a 4×7 m rectangle. From these data plus the number of shoot segments of every plant (Eq. (2)) centered at the plant location coordinates we obtain the values of matrix $V_{j,i}(x,y,t)$. The results are exemplified in Fig. 4 where we plotted together the values of the three species for level 1 (10 cm above ground).

Appendix C provides details of how we calculate matrices **V** and **K**. With these matrices, we calculate the matrix $S_{j,i}(x,y,t)$

$$S_{j,i}(x,y,t) = \int_{-\infty}^{\infty}\int_{-\infty}^{\infty} V_{j,i}(x,y,t)K_{j,i}\left(x-x',y-y'\right)dx'dy' \tag{3}$$

Numerically, this convolution was conducted over the high-resolution grid and following methods of Borse (1997)

$$S_{j,i}(x,y,t)\approx ifft2\left[fft2\left(V_{j,i}(x,y,t)\right)\circ fft2\left(K_{j,i}(x,y)\right)\right] \tag{4}$$

where *fft*2 refers to the bidimensional fast Fourier transform, *ifft*2 to the inverse bidimensional fast Fourier transform, and the symbol ∘ represents the Hadamard or entry-wise product of the two matrices. For more details see Appendix A.

Hereafter we refer to two 400×700 matrices, $\mathbf{V}_{j,i}(t)$ and $\mathbf{S}_{j,i}(t)$ for species *j* at level *i* resulting from discretization of functions $V_{j,i}(x,y,t)$ and $S_{j,i}(x,y,t)$ respectively at high-resolution. Non-zero entries of $\mathbf{V}_{j,i}(t)$ correspond to the number of shoot segments at level *i* of all plants of species *j* but lumped in the cells where plants are centered. Entries of $\mathbf{S}_{j,i}(t)$ contain the number of shoot segments in each cell for species *j* and level *i*.

Addition of the matrices $\mathbf{S}_{j,i}(t)$ across species produces a matrix $\mathbf{S}_i(t)$ of total shoot segments at level *i*. Fig. 5 exemplifies the results plotting the total number of shoot segments in each cell at level 1. We show only a 2×2 m section of the plot.

3.4. Step 4: leaf area index

To determine the amount of light transmitted downwards from one level to the next we first calculate the leaf area index (LAI) for each cell at each level. For this we gathered information in the field about the geometric arrangement of shoots (Table 4) and made some simple calculations assuming constant geometrical arrangement by level (Acevedo and Raventós, 2002). For each species *j*, we measured α_j as average shoot angle with respect to the horizontal (degrees) and w_j as average shoot width (cm). Then calculated l_j, length of shoot segments (cm) between levels, using $l_j = 10/\sin(\alpha_j)$ cm, and la_j, shoot area in cm^2 using $la_j = l_j \times w_j$. Note that because a cell is 1 cm^2, la_j is directly the contribution to LAI for that shoot.

Next we assume LAI is given by shoot surface, and used the product of la_j times the matrix $\mathbf{S}_{j,i}(t)$

$$\mathbf{A}_{j,i}(t) = la_j\mathbf{S}_{j,i}(t) \tag{5}$$

where the matrix $\mathbf{A}_{j,i}(t)$ is the LAI of species *j* in level *i*. Entries of this matrix contain the LAI for a particular cell. The total LAI in level *i* is then obtained summing over all the species

$$\mathbf{A}_i(t) = \sum_j \mathbf{A}_{j,i}(t). \tag{6}$$

3.5. Step 5: light attenuation

We need to estimate the fraction of light passing from one level to the next immediately below in order to calculate the fraction of shoot segment under direct light or shade in each level. The number of shoot segments at each level determines the number of shoots segments receiving direct light at the level immediately beneath, which decreases from top to bottom. We use exponential attenuation (Monsi and Saeki, 1953)

$$\mathbf{R}_i(t) = \mathbf{R}_{i+1}(t)\exp\left(-\sum_j \kappa_j\mathbf{A}_{j,i+1}(t)\right) \tag{7}$$

Table 3
Mean square error between the kernel model and field data for shoot segment number. These values are scaled by a 10^{-4} factor.

Species	Level									
	1	2	3	4	5	6	7	8	9	10
E	12.0	5.2	3.5	5.6	9.3	–	–	–	–	–
L	4.3	2.8	3.4	4.4	4.6	5.2	7.5	–	–	–
A	5.0	3.5	4.7	5.1	5.6	6.3	8.8	14.0	13.0	13.0

where $\mathbf{R}_i(t)$ is the fraction of radiation reaching level i from the above level $i+1$, κ_j is the light extinction coefficient for species j. We assume $\mathbf{R}_i(t)$ at top level of that cell to be 1. According to Monteith and Unsworth (1973), κ_j is given by the ratio of shaded area on the horizontal plane and the area of the shading element. Here we only consider vertically incident light on the cell, and consequently $\kappa_j = \cos\alpha_j$ which takes values 0.5, 0.34, and 0.5 for *E*, *L*, and *A* respectively. These values are close to 0.4, the value proposed by Larcher (2003) for grasses.

Values of the entries of matrix $\mathbf{R}_i(t)$ range from 0 to 1, being equal to 1 at the top of the level occupied at the cell and decreasing as a function of number of shoot segments at each level. For each cell subtracting the corresponding $\mathbf{R}_i(t)$ entry from 1 gives us the fraction of incident radiation attenuated by the canopy.

3.6. Step 6: number of shoots segments under shade

Now we will assume that the fraction of incident light reaching a cell is available all over that cell and that shoot segments of that cell are exposed uniformly to that fraction of light. Then, entry-wise multiplication of matrices $\mathbf{R}_i(t)$ and $\mathbf{S}_{j,i}(t)$ gives the number of shoot segments by species and level that receive light

$$\mathbf{P}_{j,i}(t) = \mathbf{R}_i(t) \circ \mathbf{S}_{j,i}(t). \tag{8}$$

Also we form a matrix $\mathbf{Q}_{j,i}(t)$ with entries $q_{j,i}^{kx,ky}(t)$ given by

$$q_{j,i}^{kx,ky}(t) = 1 - p_{j,i}^{kx,ky}(t) \tag{9}$$

where $p_{j,i}^{kx,ky}(t)$ is the entry of $\mathbf{P}_{j,i}(t)$ at row kx and column ky.

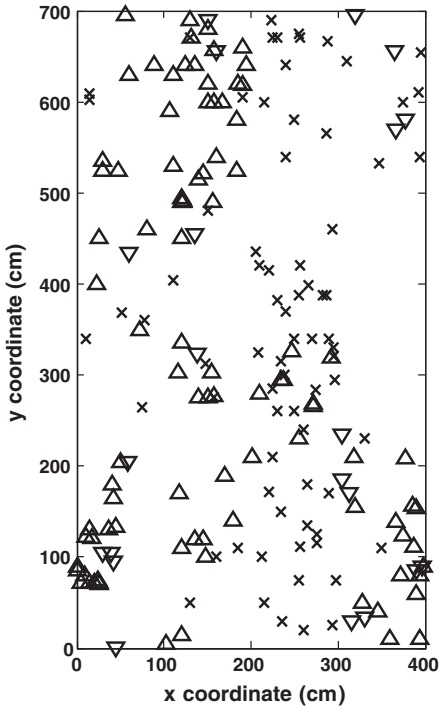

Fig. 3. Spatial distribution of the plants from a field rectangular plot of size 400×700 cm. Symbols are: *A*: X; *E*: ▽; *L*: Δ.

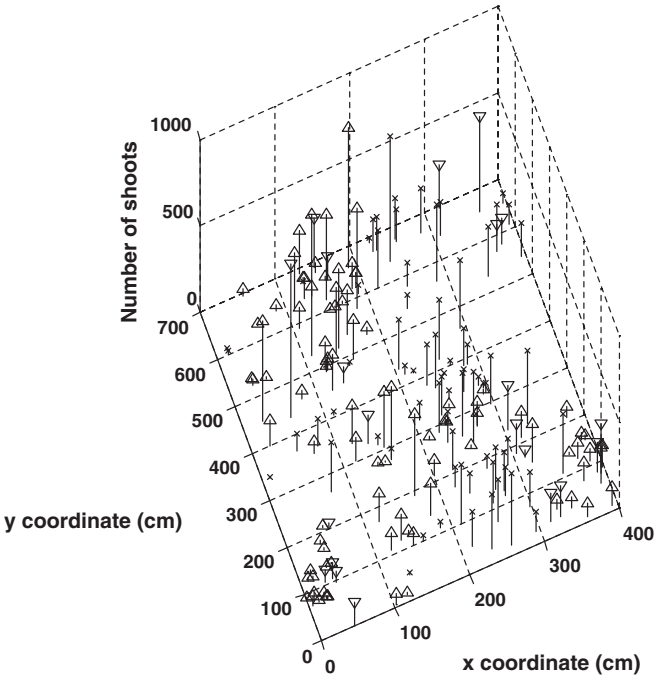

Fig. 4. Number of shoots at level 1 for the three species from the three matrices $\mathbf{V}_{j,1}$ using the plant location information in Fig. 3. Symbols are: *A*: X; *E*: ▽; *L*: Δ.

Now, the total number of shoots segments of species j that receive direct radiation and are transpiring is

$$\mathbf{P}_j(t) = \sum_{i=2}^{mj} \mathbf{P}_{j,i}(t) \tag{10}$$

where, as defined earlier, m_j is number of 10 cm-levels reached by plants of the species j, and the first level $i=1$ is excluded from the summation because shoots are non-photosynthetically active at this level (Raventós et al., 2004). Also the total number of shoot segments of species j that are in the shade and transpire is

$$\mathbf{Q}_j(t) = \sum_{i=2}^{mj} \mathbf{Q}_{j,i}(t). \tag{11}$$

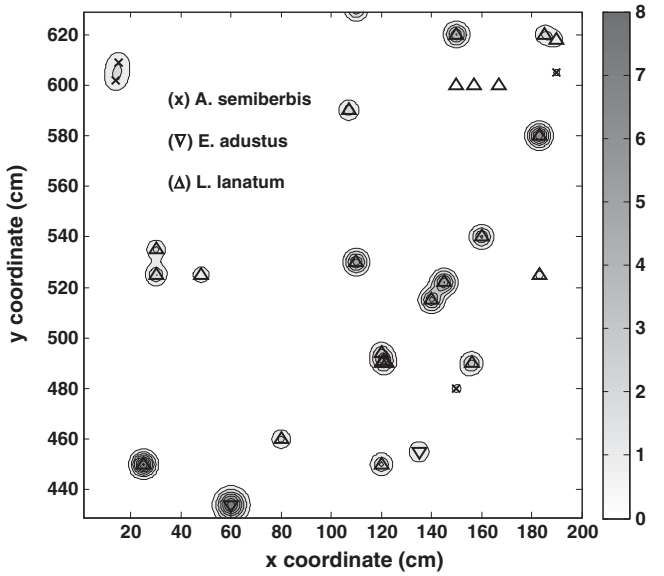

Fig. 5. Actual distribution of shoot segments in space as given by the matrices $\mathbf{S}_{j,1}$ at level 1. We show only a 2×2 m section of the plot. Each mound shows how the shoot segments depicted in Fig. 4 share the space.

Table 4
Geometric arrangement of shoots (used to calculate LAI) and maximum daily transpiration rates. Transpiration rates were measured in April, 2006. $T_{j,l}$ is rate under light and $T_{j,s}$ is rate under shade.

Geometry					Transpiration (cm day^{-1})	
Species	α_j (°)	w_j (cm)	l_j (cm)	la_j (cm^2)	$T_{j,l}$	$T_{j,s}$
E	60	0.33	11.54	3.48	0.24	0.06
L	70	0.32	10.64	3.41	0.38	0.12
A	60	0.67	11.54	7.06	0.17	0.10

Fig. 6 shows the frequency of shaded shoot segments per plant at level 1. We show only a 2×2 m section of the plot.

3.7. Step 7: evapotranspiration rate

Transpiration rate depends on several factors. We work here with the maximum transpiration rate for each species achieved when soil water content is at field capacity. Using $\mathbf{P}_j(t)$ and $\mathbf{Q}_j(t)$ we calculate the maximum transpiration rate for each species j in each cell according to:

$$\mathbf{T}_j(t) = \left(\mathbf{P}_j(t)T_{j,l} + \mathbf{Q}_j(t)T_{j,s}\right)la_j \times 10^{-4} \quad (12)$$

where $T_{j,l}$ and $T_{j,s}$ are measured maximum transpiration rates of shoot segments of species j growing under light or under shade respectively (Table 4), la_j is the area of the shoot segments we calculated before (Table 4), and the 10^{-4} factor is to convert cm^2 to m^2 (Table 4). Total maximum transpiration rate is obtained by summing over all the species that occupy each cell

$$\mathbf{T}_{\max}(t) = \sum_j \mathbf{T}_j(t). \quad (13)$$

We assume that maximum evaporation rate from the soil (E_{max}) under direct sunlight averages to 0.15 cm day^{-1} and 0 under shade. To determine how much light reaches each cell on the soil we use the matrix $\mathbf{R}_1(t)$ which is the fraction of radiation reaching level 1 calculated from Eq. (7).

$$\mathbf{E}_{\max}(t) = 0.15\mathbf{R}_1(t) \quad (14)$$

We neglect the shade created by level-1 shoots, which results in a slight overestimation of soil evaporation.

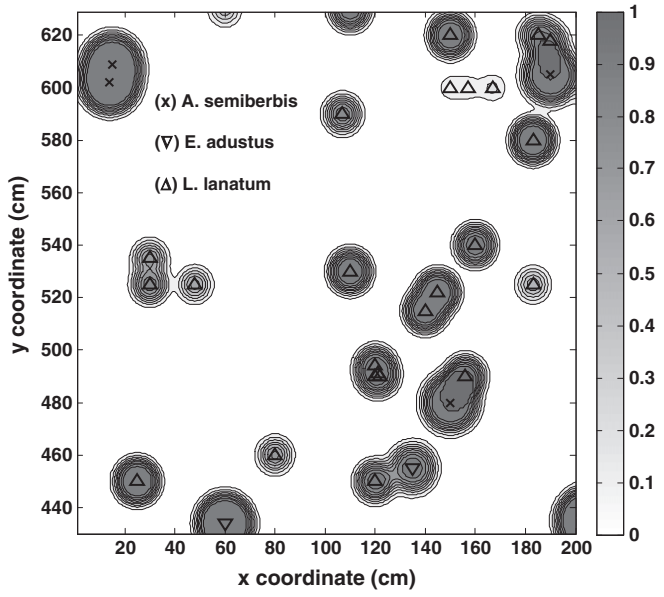

Fig. 6. Frequency of shaded shoot segments per plant at level 1. Frequencies are closer to 1 at level 1 since this level is at the base of the plant. We show only a 2×2 m section of the plot.

Table 5
Number of shoots at base level and biomass (dry weight) measurements (five replicates) to calibrate the average relation of number of shoot segments to biomass. Measurements conducted in April, 2006.

Species	Measured		Estimated	
	Shoots	Biomass (g)	Biomass (g)/shoot	Biomass (g)/segment
E	154, 187, 350, 368, 381	75, 125, 140, 148, 213	0.50 ± 0.11	0.40 ± 0.12
L	94, 134, 150, 188, 210	56, 57, 58, 94, 95	0.46 ± 0.08	0.26 ± 0.09
A	47, 67, 72, 82, 95	46, 80, 100, 136, 137	1.33 ± 0.26	0.31 ± 0.06

Next, we aggregate entries of the high-resolution matrices $\mathbf{E}_{\max}(t)$ and $\mathbf{T}_{\max}(t)$ to the quadrat level. Recall that there are 100×100 cells in a quadrat. We form matrices $\mathbf{E}_{\max}(t)$ and $\mathbf{T}_{\max}(t)$ whose entries $E^{ix,iy}_{\max}(t)$ and $T^{ix,iy}_{\max}(t)$ are obtained summing all entries of matrices $\mathbf{E}_{\max}(t)$ and $\mathbf{T}_{\max}(t)$ respectively that belong to a quadrat of row *ix*, column *iy*.

3.8. Step 8: soil moisture balance

At this point we calculate soil moisture $s_{ix,iy}(\tau)$ in the quadrat of row *ix*, column *iy* at time τ. Here we use τ to distinguish time at the daily scale from time t at the monthly scale. Variable $s_{ix,iy}(\tau)$ is relative soil water content in relation to saturation level (dimensionless). Following Segarra et al. (2009), we write the balance of $s_{ix,iy}(\tau)$ as the difference between infiltration and loss rates (Laio et al., 2001)

$$\eta Z\frac{ds_{ix,iy}(\tau)}{d\tau} = I\left(s_{ix,iy}(\tau)\right) - L\left(s_{ix,iy}(\tau)\right) - E\left(s_{ix,iy}(\tau)\right) - T\left(s_{ix,iy}(\tau)\right) \quad (15)$$

where, η: porosity of soil (dimensionless, 0.42), Z: depth of soil (30 cm), $I(s_{ix,iy}(\tau))$: soil infiltration rate (cm day^{-1}), $L(s_{ix,iy}(\tau))$: soil water loss rate by leakage or deep percolation, $E(s_{ix,iy}(\tau))$: soil water loss rate by evaporation, and $T(s_{ix,iy}(\tau))$: transpiration rate. All rates are given in cm day^{-1} and will be explained next. We assume that there is no horizontal transport of water in the soil. In Appendix D we explain how to calculate the terms of Eq. (15).

Initial conditions for the first day, month, and year of the simulation $s_{ix,iy}(0)$ were assigned the value 0.2 for all quadrats, which is April's soil moisture according to Segarra et al. (2009).

After obtaining the daily soil water content, $s_{ix,iy}(\tau)$ from Eq. (15) for each month we average the values to obtain a monthly average $\bar{s}_{ix,iy}(t)$. This is then used to calculate the rate of shoot production and mortality for each species j in the following manner.

When soil moisture is lower than the point below which plants begin closing their stomata (s^*), shoot production rate starts to decrease linearly. When the soil moisture drops below the wilting point (s_w), mortality increases from 0. Details are explained in Appendix E.

The new values of shoot production and mortality are then substituted in Eq. (1) to obtain the new number of shoots $n^1_{j,k}(t)$ and repeat the monthly cycle.

3.9. Step 9: biomass

To build a relationship of shoots to biomass, in April 2006 we measured number shoots at basal level and biomass of five individuals of each species (replicates). The measurements are reported in the first two columns of Table 5. Biomass per shoot can be calculated by replicate, the average and standard deviation is reported in the third column of Table 5.

However, not all shoots are the same size and in order to account for vertical structure we proceed as follows. The number of shoot segments by level is projected from base level using Eq. (2), and matrices $\mathbf{M}_j$, assuming sequences of emergence $\rho^1_{j,k}(t+1)$ ratio at base level calculated as explained in Appendix B for fixed differences $n^1_{j,k}(t+1) - n^1_{j,k}(t)$ at all t of 80, 30, and 10 for *E*, *L*, and *A* respectively (values reported in Raventós et al., 2004). The vertical structure of

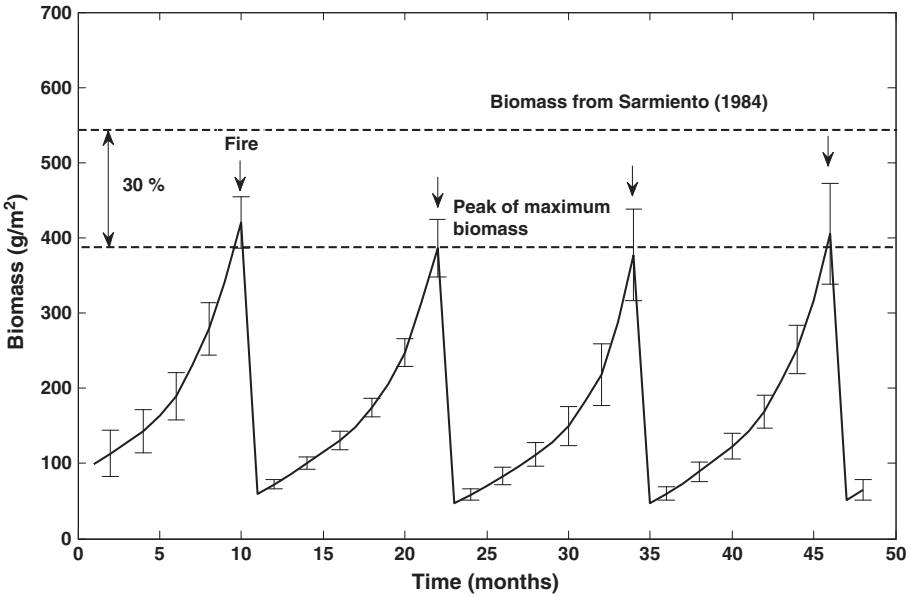

Fig. 7. Model output showing changes in community biomass throughout time. Annual peaks of biomass are compared to biomass estimated from Sarmiento (1984).

shoot segments for each replicate is calculated by interpolating the measured value of number of shoots at base level, and the numbers of shoot segments are summed across vertical levels for each replicate. Then, measured biomass of the replicate is divided into this number of shoot segments to obtain biomass per shoot segment. Average and standard deviation of biomass per segment (g/segment) across replicates are calculated and reported in the last column of Table 5. Now we denote these average values as coefficients bm_j for each species j.

Finally in each month we multiply scalar bm_j by matrix $\mathbf{S}_{j,i}(t)$ of number of shoot segments at level i of all plants of species j generated in step 3 to estimate $\mathbf{B}_{j,i}(t)$ biomass (dry weight in g) by species and level.

$$\mathbf{B}_{j,i} = bm_j \mathbf{S}_{j,i}(t) \tag{16}$$

To evaluate the model we compared biomass to the values reported in Sarmiento (1984). For this purpose, we conducted five 5-year simulation runs. Each 5-year run starts in April with initial conditions explained above. It was observed that the pattern of monthly dynamics are repeated after the first year, therefore year 1 was dropped from all run results to remove transient behavior. As shown in Fig. 7, we compared the annual variation of the peak average biomass per square meter from the model over years 2–5 (48 months) of simulation with the maximum biomass estimated in the field for a similar community (Sarmiento, 1984).

3.10. Step 10: mortality by fire

If the current simulated month is a fire-prone month (end of dry season), then there is fire-produced mortality of a fraction of the shoots. Therefore, each February, the model kills 90% of the shoots segments of all species (Segarra et al., 2009). Although fire intensity varies from year to year, we do not include this variability and work with only an average of 90% because fire is the leading cause of mortality among the grasses of the savanna (Silva and Castro, 1989). Therefore the peak biomass calculated in Step 9 is always the one corresponding to the month of February just before the fire.

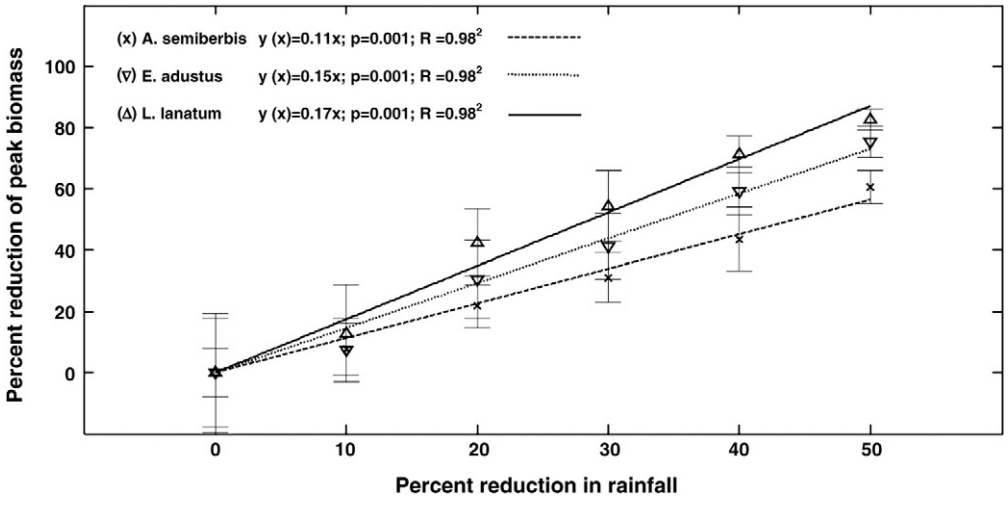

Fig. 8. Changes in peak biomass along a gradient of annual rainfall using scenarios of % rainfall reduction, from 0% (precipitation = 1250 mm/year) to 50% (precipitation = 625 mm/year). The slope of the regression line indicates the species' sensitivity to drought.

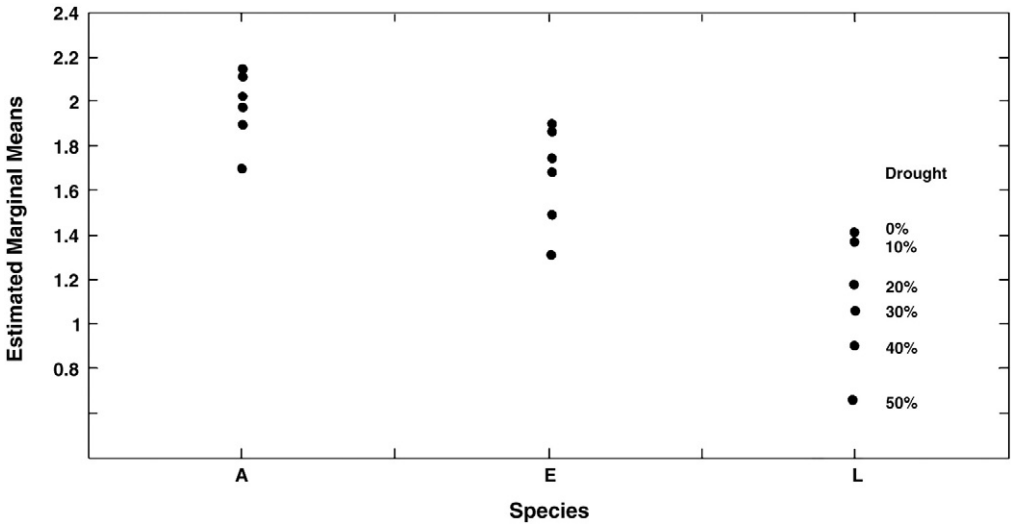

Fig. 9. Estimated marginal means of log transformed peak biomass to analyze interactions in ANOVA analysis of drought scenarios by species.

4. Drought simulations

According to Dai (2010) rainfall in the area will decrease by 20% during this century due to climate change, one of the largest expected decreases worldwide. Because this is an uncertain number we explored scenarios {0, 10, 20, 30, 40, 50%} encompassing the expected 20% change, including an intense drought scenario of 50%. Monthly values H_m, H_{sd}, and J_m given in Table 1 were used for the base scenario (0% reduction). For all other scenarios, generated daily rainfall per Step 8 was reduced by the corresponding percentage. We reduced only the amount of rain in a rain day and not the number of rain days in a month.

We conducted five year simulation runs for each scenario. Each 5-year run starts in April with initial conditions explained above. The daily rain sequence of each run for the base scenario uses a different seed of the random number generator. Then the daily rain sequence of the base scenario was reduced by 10, 20, 30, 40, and 50% to obtain the daily rain sequence of the drought scenarios. For each run we calculate the total plot peak biomass per species at the end of the fifth simulation year. Then for each scenario, we calculated the mean and standard deviation of the 5th-year total plot peak biomass per species of the five runs.

5. Results

In order to evaluate this model we have applied it to a savanna community, using actual plant distribution in a study plot (Fig. 3) and calculating the spatial (vertical and horizontal) distribution of shoot segments and plant biomass in that community (Figs. 4–7). The evaluation was made by comparison of the maximum biomass from field data and from the model's output (Fig. 7).

The responses of the three species to the scenarios of increasing drought are shown in Fig. 8. The comparison is made on the basis of percent reduction of peak biomass with respect to the base scenario. We calculated regression lines with zero intercept for each species using the mean of the runs for each scenario. The slopes of the regression lines obtained are 0.15, 0.17 and 0.11 in%/% for *E*, *L* and *A* indicating that *A* is the most drought resistant, followed by *E*, and that *L* is the least resistant. A two-way ANOVA shows that there is a significant difference in slope among species ($F=1030.37$; $p<0.001$) and drought scenarios ($F=130.50$; $p<0.001$).

However, interaction between species and draught level is also significant ($F=4.455$; $p<0.001$). Fig. 9 shows that there are significant differences for all drought levels except scenarios of 0 and 10% rainfall reduction. Species *A* is the least affected by drought because its estimated marginal means are higher and have lower range of variation. On the contrary, species *L* is the most affected by drought because its estimated marginal means have lower values and have higher variability. Finally, species *E* is intermediate between *L* and *A*.

A posteriori pairwise comparisons of means using the Student-Neuman-Keuls (SNK) statistic for the three species show significant differences among species, with *A* the least affected by drought (2.18), followed by *E* (1.89), and by *L* (1.31). Similarly, pairwise comparisons by drought level using SNK show that drought scenarios of 50, 40, 30 and 20% (with 1.45, 1.64, 1.79, and 1.87 respectively) are homogeneous and independent but the 10% and the 0% (no reduction) scenarios are not (with 2.00 and 2.04 respectively). Therefore, reductions of 10% or lower do not have significant effects on peak biomass.

6. Discussion

In this paper, we have developed a model using matrices and convolution techniques, in order to simulate light incidence and transpiration rates of a vegetation community of the savannah. With this model, we have explored the effects of drought on these plants. Our model suggests that drought resistance increases with the biomass/transpiration ratio for the species considered.

The first objective of this work was to incorporate shoot vertical distribution, light incidence and transpiration rates into our previous model (Segarra et al., 2009; Segarra et al., 2010). The model presented in this paper developed using matrices and convolution techniques, achieves this objective. Including shade in vegetation modeling is important because it accounts for potential effects on ecophysiological processes that depend on light (Pearcy and Yang, 1996) and potential effects on plant morphology (Sekimura et al., 2000). The problem, as discussed in the introduction, is that it is difficult to develop a model that can be easily applied to large surfaces and on a daily basis, while taking into account the structure of plants involved calculating the shading between stems.

To resolve this problem different models have been proposed. De Castro and Fetcher (1998) divided the canopy into cubic cells, each one characterized by mean leaf angle and the leaf area index. Although this model is similar to ours, it has the drawback that it is computed cell by cell, making it more computer-intensive. Sinoquet et al. (2000) propose a simulation model of light partitioning in horizontally homogeneous multispecies canopies. However this model only takes into

account the diffuse radiation, so it could only be applied to overcast sky conditions. Rosati et al. (2001) use the partitioning of leaf area into one of six classes to estimate canopy light interception and absorption. The drawback is that this approach only could be advantageous in crops where spacing is regular and plant material is genetically uniform, thus it is not applicable in heterogeneous media. Finally, Oyarzun et al. (2007) develop a model of shading from trees and orchids, considering trees as prismatic-shaped porous bodies, so it replaces the actual shape of the tree by a regular geometric figure and, furthermore, shading is calculated tree by tree.

Our model, by contrast, uses direct solar radiation, it can be applied to plant communities with any spatial distribution and different morphologies, and it need not calculate each individually spatial unit, because the convolution technique treats all plants of the same species pooled in compartments instead of performing individual calculations for each plant. This improves calculation speed while preserving architectural detail.

To calculate soil moisture we have followed the same procedure as Guswa et al. (2002), assuming that there is a linear relation between evapotranspiration and soil moisture. To determine the effect of soil moisture on plant growth we followed an approach similar to Porporato et al. (2001), who define a constant stress following the same equation of transpiration given by Guswa et al. (2002). We use the same equation given in Porporato et al. (2001), but substituting the constant stress by one dependent on shoot production rate. Thus our equations for shoot production and transpiration are similar. We have added a new Eq. (E2) that calculates shoot mortality when soil moisture is below the hygroscopic point.

The evaluation of our model, made by comparison of the maximum biomass from field data and from the model's output (Fig. 7), shows that the model underestimates total biomass by 30% because we modeled only three species of this community. According to Sarmiento (1983) these three species may represent about a 70% of the total biomass in this particular community, therefore we can account for this 30% underestimation.

Our second objective was to explore the effects of drought on the plant community. As expected, the three species respond differently to the drought scenarios except for the base and 10% rainfall reduction scenarios. The lesser the slope in Fig. 8 the less pronounced is the relative decrease in biomass, indicating more resistance to drought. The slope for *A* (0.11) is the lowest of the three, suggesting that this species is more drought resistant, *L* has the highest slope (0.17), suggesting that it may be the least resistant, and *E* is intermediate in value (0.15). Four factors interact in the model to determine species differences in drought resistance of peak biomass: shoot production rate, proportion of shaded shoots, shoot biomass, and transpiration rate. In fact, the ratio of shoot biomass to transpiration weighted by proportion of shaded shoots is 4.76, 1.96, 10.28 for *E*, *L* and *A* which are inversely aligned with the slopes 0.15, 0.17, 0.11 for *E*, *L* and *A*. The larger the biomass/transpiration ratio the slope is lower and the species is more drought resistant.

These results are in agreement with reports from the literature indicating that *L* is less adapted to dry conditions (Sarmiento, 1983; Silva and Sarmiento, 1976), than *A* and *E* which are present in drier conditions. Although there is not conclusive evidence, this differential resistance to drought has been related to the growth phenology of the grass species (Silva, 1987). Species starting growth before the onset of rains (like *E*) or toward the end of the rain season (like *A*) should be more resistant to drought than those species growing during the rainy season (like *L*).

Additionally, *A* and *E* have higher proportion of biomass allocated to leaves than *L* (Table 5), and this may increase their ability to grow in savannas. This allocation factor has been proposed as one of the main features contributing to a high competitive potential (Baruch and Bilbao, 1999; Baruch et al., 1989; Bilbao and Medina, 1990; Hodgkinson et al., 1989; Williams and Black, 1994).

The results of our model are also consistent with field measurements made by one of us (Garcia-Nunez, personal communication), showing that *A* closes stomata when the light radiation is high and hence higher evaporative demands and open when radiation is low, resulting in similar transpiration rates in both cases. Conversely *L* was less responsive to changes in radiation load in terms of stomatal conductance, maintaining the stomata partially closed along the days, which in turn determine that transpiration rates depend more in evaporative demand. *E* showed an intermediate response.

The lack of significant peak biomass response for 10% rainfall reduction or lower is due to the assumptions underlying model Eq. (E1) determining shoot production decrease as a function of soil moisture. We have assumed that shoot production is only affected when soil moisture goes below s^*(soil moisture level below which plants begin closing their stomata), and this critical level is not reached by smaller reductions of rainfall.

Two major differences among species that can affect response to drought are not included in our model. One is underground/aerial biomass ratio, which is high in *L* and *E* (2 to 5) and low in *A* (0.1) (Goldstein and Sarmiento, 1987; Silva, 1987). The other is differential responses to soil water stress since we have used the same values of parameters s_h, s_w y s^* for all species as in Laio et al. (2001).

7. Conclusions

We have demonstrated that the integrated use of convolution, transition matrices, shading calculations, and soil moisture balance allows to model aboveground processes of savanna communities. The advantages of this technique are that it simplifies the simulation of plants with complex structures; the sensitivity analysis of the transition matrix can draw conclusions on the dynamics of growth; finally it increases the computational speed in the case of plant with complex structures and high density, which is important to explore a variety of scenarios, such as drought or fires.

The model is applicable to other types of plant communities once we include corresponding plant traits such as growth phenology and architecture. Although we have used a matrix model is not a requirement. This technique can be applied to any plant growth model, provided to calculate the intersection of each shoot in each vertical level. There are several processes that can be included to improve this model: 1) photosynthetic rates to determine production and growth, 2) daily variations in the angle of light incidence, and 3) species-specific values for soil water stress parameters s_h, s_w and s^*.

Acknowledgments

We thank the Spanish Ministry of Education and Science (CGL2007-65315-C03 02; CGL2008-05112-C02-01/CLI) and GA-LC-031/2010 funded by CGA-La Caixa for their financial assistance.

Appendix A

Convolution is a mathematical operator that transforms two functions, *f* and *g*, into a third function, which in a certain sense represents the magnitude in which *f* and a shifted version of *g* are superimposed. Convolution is a very general type of moving average, as can be seen if one of the functions is taken as the characteristic function of an interval.

The convolution of *f* and *g* is denoted as f^*g. It is defined as the integral of the product of both functions where one of them is shifted by τ.

$$f(t) * g(t) = \int f(\tau) g(t-\tau) d\tau \quad \text{(A1)}$$

Our model uses convolution to calculate the spatial distribution of the shoots of a set of plants. This is needed because the matrix model

calculates the position of all the shoots of the plant in the central axis, and we need to know how they are distributed spatially. The advantage of this technique is that it is not necessary to calculate the individual distribution of each plant, but a single calculation will provide this for all plants within the same species. In this case, function $f(t)$ of Eq. (A1) corresponds to the shoot dispersal kernel, which measures the normal distribution of the shoots from the central axis of each plant. Our model supposes a Gaussian kernel, which means that shoot density is more intense in the central axis of the plant (the point from which the stem starts), and becomes less intense toward the edge of the plant. Convolution is only applied to plants of the same species, as each species has a different shoot structure, and therefore a characteristic kernel. Function $g(t)$ is formed by a set of segments distributed on the plane. The position of each segment on the plane reproduces the position of each plant in the model domain, and the height of each segment measures the number of shoot segments for each plant.

We use numerical methods to solve Eq. (A1). A description of how to implement these calculations using MATLAB is given below. This program shows how to apply this technique to two-dimensional surfaces. The text after the% sign are comments that do not affect execution of the program.

```
%**************************************
% Two-dimensional model with several elements
% Plot consists of 128×128 points
% Values range between −10 to +10 function; convolution2d
np = 128;
xl = 10; dx = 2*xl/np;
x = linspace(−xl,xl − dx,np);
[X,Y] = meshgrid(x,x);
% Set initial conditions for six plants. Numbers in parentheses are
% plant coordinates. P is number of shoot segments of each plant
P(56,20) = 5;
P(50,38) = 1;
P(22,80) = 3;
P(27,40) = 7;
P(90,78) = 8;
P(110,110) = 5;
% Defines dispersal kernel
D = 2;
K = 1/(2*pi*D^2)*exp(−(X.^2 + Y.^2)/(2*D^2));
% Obtains the Fourier transform of matrix P and the dispersal
% kernel.
fP = fft2(P);
fK = dx.^2*fft2(K);
% The two matrices obtained in the previous step are multiplied
% entry-wise.
Pt = real(fftshift(ifft2(fP.*fK)));
% The dispersed distribution is normalized
numPt = dx^2*trapz(trapz(Pt));
Pt = numP/numPt*Pt;
% Graph
surf(x,x,Pt)
xlabel('Axis x')
ylabel('Axis y')
zlabel('Frequency of shoot segments')
%**************************************
```

Appendix B

The vectors $\mathbf{n}_{j,k}(t)$ and $\boldsymbol{\rho}_{j,k}(t+1)$ are $m_j \times 1$, where m_j is number of vertical levels reached by plants of the species, $m_E = 5$, $m_L = 7$, and $m_A = 10$ for E, L and A respectively. Matrix $\mathbf{M}_j$ is $m_j \times m_j$. The transition matrices for species E, L, and A are (Raventós et al., 2004):

$$M_E = \begin{bmatrix} 1 & 0 & 0 & 0 & 0 \\ .18 & .82 & 0 & 0 & 0 \\ 0 & .44 & 56 & 0 & 0 \\ 0 & 0 & 39 & .61 & 0 \\ 0 & 0 & 0 & .07 & .93 \end{bmatrix}$$

$$M_L = \begin{bmatrix} 1 & 0 & 0 & 0 & 0 & 0 & 0 \\ .24 & .76 & 0 & 0 & 0 & 0 & 0 \\ .096 & .9 & .004 & 0 & 0 & 0 & 0 \\ 0 & .03 & .52 & .45 & 0 & 0 & 0 \\ 0 & 0 & 0 & .4 & .6 & 0 & 0 \\ 0 & 0 & 0 & 0 & .22 & .78 & 0 \\ 0 & 0 & 0 & 0 & 0 & .07 & .93 \end{bmatrix}$$

$$M_A = \begin{bmatrix} 1 & 0 & 0 & 0 & 0 & 0 & 0 & 0 & 0 & 0 \\ .25 & .75 & 0 & 0 & 0 & 0 & 0 & 0 & 0 & 0 \\ 0 & 1.78 & .11 & 0 & 0 & 0 & 0 & 0 & 0 & 0 \\ 0 & .32 & .84 & 0 & 0 & 0 & 0 & 0 & 0 & 0 \\ 0 & 0 & .37 & .63 & 0 & 0 & 0 & 0 & 0 & 0 \\ 0 & 0 & 0 & .66 & .34 & 0 & 0 & 0 & 0 & 0 \\ 0 & 0 & 0 & .03 & .97 & 0 & 0 & 0 & 0 & 0 \\ 0 & 0 & 0 & 0 & .27 & .73 & 0 & 0 & 0 & 0 \\ 0 & 0 & 0 & 0 & 0 & .51 & .49 & 0 & 0 & 0 \\ 0 & 0 & 0 & 0 & 0 & 0 & .89 & .1 & .01 & 0 \end{bmatrix}$$

The $\boldsymbol{\rho}_{j,k}(t+1)$ ratio of shoot emergence and mortality is first calculated at level 1

$$\rho^1_{j,k}(t+1) = \frac{n^1_{j,k}(t+1)}{n^1_{j,k}(t)} \tag{B1}$$

And then at all other levels $i = 2, \ldots, m_j$

$$\rho^i_{j,k}(t+1) = \begin{cases} \rho^1_{j,k}(t+1) & \text{when } \rho^1_{j,k}(t+1) \le 1 \\ 1 & \text{when } \rho^1_{j,k}(t+1) > 1 \end{cases} \tag{B2}$$

The first entry $\rho^1_{j,k}(t+1)$ of the ratio vector is calculated from the change of the total number of shoots $n^1_{j,k}(\cdot)$ from time t to time $t+1$, calculated in Section 3.1, according to Eq. (1).

Appendix C

The three species have the same growth pattern, similar to an inverted cone whose diameter increases upwards, but the species differ in rate of change of diameter as they grow up. Based on this we used a Gaussian bidimensional distribution for the kernel $K_{j,i}(x,y)$ for level i and species j, given by

$$K_{j,i}(x,y) = \frac{1}{2\pi {D_{j,i}}^2} \exp\left(\frac{-\left(x^2+y^2\right)}{2{D_{j,i}}^2}\right) \tag{C1}$$

where $D_{j,i}$ measures the dispersion coefficient for species j and level i.

We use an empirical power function to calculate the coefficient $D_{j,i}$ for each level i, being lowest at the base and increasing with height

$$D_{j,i} = c_j\left(i + d_j\right)^{f_j} \tag{C2}$$

The parameter values for each species were obtained by matching field data of shoot segments distribution at each level (Table 2).

With the kernel for shoot segment distribution, we now horizontally distribute the number of shoot segments assuming that plant k is located at point (x_k, y_k). We use the first set of data from the field with the coordinates of each plant position in a 4×7 m rectangle

(Fig. 3) to define a 2D function for each species j and level i at time t

$$V_{j,i}(x,y,t) = \sum_k n^i_{j,k}(t)\delta(x-x_k, y-y_k) \tag{C3}$$

by summing over all plants k of species j a set of Dirac delta functions with intensities given by the number of shoot segments and centered at the plant location coordinates. The results are exemplified in Fig. 4 where we plotted together the values of the three species for level 1 (10 cm above ground).

Appendix D

Rainfall of the day $h(\tau)$ in cm day^{-1} is randomly generated using an exponential distribution function for each month t, according to the mean monthly precipitation, and the average rainfall for rainy days of each month t (Segarra et al., 2009).

Frequency of rainy days in each month $j_m(t)$ is calculated as a ratio of $J_m(t)$, number of days with rain in the month m, to the number of days in that month (Table 1). Then, the ratio of $H_m(t)$, the average rainfall in the month m, to $J_m(t)$ for the same month gives the average rainfall for every rainy day of the t month, $H_d(t)$, in cm day^{-1}. This is to say, $H_d(t) = \frac{H_m(t)}{J_m(t)}$. Then, for each day τ of the t month, we generated a random number rn uniformly distributed on [0,1]. If $rn > j_m(t)$, there is no precipitation and then $h(\tau) = 0$. Otherwise if $rn \le j_m(t)$, there is precipitation on that day, and the amount $h(\tau)$ is calculated generating an exponentially distributed random number with cumulative $F(h) = 1 - \exp(-h(\tau)/H_d(k))$.

Canopy interception rc, with a value 0.05 cm day^{-1} as in Segarra et al. (2009), is subtracted from the rainfall to obtain effective rainfall

$$h_e(\tau) = h(\tau) - rc \tag{D1}$$

We assume the same value $h_e(\tau)$ for all quadrats. Soil infiltration rate is calculated from the effective rainfall but limited by the deficit $(1-s)\eta Z$ for larger amounts of rainfall

$$I\left(s_{ix,iy}(\tau)\right) = \begin{cases} 0 & for \quad h_e(\tau) \le 0 \\ h_e(\tau) & for \quad 0 < h_e(\tau) < \left(1-s_{ix,iy}(\tau)\right)\eta Z \\ \left(1-s_{ix,iy}(\tau)\right)\eta Z & for \quad h_e(\tau) \ge \left(1-s_{ix,iy}(\tau)\right)\eta Z \end{cases} \tag{D2}$$

The next equations (D3)–(D5) are from Guswa et al. (2002). The loss terms are calculated as

$$L\left(s_{ix,iy}(\tau)\right) = K_s \left(\frac{\exp\left(\beta\left(s_{ix,iy}(\tau) - s_{fc}\right) - 1\right)}{\exp\left(\beta\left(1-s_{fc}\right) - 1 \right.} \quad s_{fc} < s_{ix,iy}(\tau) < 1 \right. \tag{D3}$$

$$E\left(s_{ix,iy}(\tau)\right) = \begin{cases} 0 & for \quad 0 < s_{ix,iy}(\tau) \le s_h \\ E^{ix,iy}_{\max}(t)\dfrac{s_{ix,iy}(\tau) - s_h}{s^* - s_h} & for \quad s_h < s_{ix,iy}(\tau) \le s^* \\ E^{ix,iy}_{\max}(t) & for \quad s^* < s_{ix,iy}(\tau) \le 1 \end{cases} \tag{D4}$$

$$T\left(s_{ix,iy}(\tau)\right) = \begin{cases} 0 & for \quad 0 < s_{ix,iy}(\tau) \le s_w \\ T^{ix,iy}_{\max}(t)\dfrac{s_{ix,iy}(\tau) - s_w}{s^* - s_w} & for \quad s_w < s_{ix,iy}(\tau) \le s^* \\ T^{ix,iy}_{\max}(t) & for \quad s^* < s_{ix,iy}(\tau) \le 1 \end{cases} \tag{D5}$$

where K_s: hydraulic conductivity at saturation (100 cm day^{-1}), β: parameter defining the exponential relationship between soil moisture and hydraulic conductivity (dimensionless, 12.7), s_{fc}: soil field capacity (dimensionless, 0.52), s_h: hygroscopic point (dimensionless, 0.08), s_w: permanent wilting point, (dimensionless,0.11), and s^*: soil moisture level below which plants begin closing their stomata (dimensionless, 0.31). In addition: $E^{ix,iy}_{\max}(t)$: maximum evaporation rate (cm day^{-1}) for the month t, $T^{ix,iy}_{\max}(t)$: maximum transpiration rate (cm day^{-1}) for the month t. Recall that these last two quantities are calculated in step 7.

Appendix E

When soil moisture is lower than the point below which plants begin closing their stomata (s^*), shoot production rate starts to decrease linearly, becoming equal to zero when moisture reaches the wilting point (s_w),

$$b_j\left(\bar{s}_{ix,iy}(t)\right) = \begin{cases} 0 & for \quad \bar{s}_{ix,iy}(t) < s_w \\ b_{j\max}\left(\dfrac{\bar{s}_{ix,iy}(t) - s_w}{s^* - s_w}\right) & for \quad s_w \le \bar{s}_{ix,iy}(t) \le s^* \\ b_{j\max} & for \quad \bar{s}_{ix,iy}(t) > s^* \end{cases} \tag{E1}$$

where $b_{j\ max}$ is the rate corresponding to water above s^* for species j.

When the soil moisture drops below the wilting point (s_w), mortality increases from 0 in proportion to the difference $(s_w - \bar{s})$,

$$\mu_j\left(\bar{s}_{ix,iy}(t)\right) = \begin{cases} 0 & for \quad \bar{s}_{ix,iy}(t) > s_w \\ \mu_{j\max}\left(\dfrac{s_w - \bar{s}_{ix,iy}(t)}{s_w - s_h}\right) & for \quad s_h < \bar{s}_{ix,iy}(t) \le s_w \\ \mu_{j\max} & for \quad \bar{s}_{ix,iy}(t) = s_h \end{cases} \tag{E2}$$

where $\mu_{j\ max}$ is the mortality rate corresponding to water below s_h for species j.

References

Accatino, F., De Michele, C., Vezzoli, R., Donzelli, D., Scholes, R., 2010. Tree–grass coexistence in savanna: interactions of rain and fire. Journal of Theoretical Biology 267, 235–242.

Acevedo, M.F., Raventós, J., 2002. Growth dynamics of three tropical savanna grass species: an individual-module model. Ecological Modelling 154, 45–60.

Alexandersson, H., 1986. A homogeneity test applied to precipitation data. Journal of Climatology 6, 661–675.

Aranda, I., Castro, L., Pardos, M., Gil, L., Pardos, J.A., 2005. Effects of the interaction between drought and shade on water relations, gas exchange and morphological traits in cork oak (*Quercus suber* L.) seedlings. Forest Ecology and Management 210, 117–129.

Ashton, M.S., Singhakumara, B.M.P., Gamage, H.G., 2006. Interaction between light and drought affects performance of tropical tree species that have differing topographic affinities. Forest Ecology and Management 221, 42–51.

Barbier, N., Couteron, P., Lefever, R., Deblauwe, V., Lejeune, O., 2008. Spatial decoupling of facilitation and competition at the origin of gapped vegetation patterns. Ecology 89 (6), 1521–1531.

Baruch, Z., Hernández, A.B., Montilla, M.G., 1989. Dinámica del crecimiento, fenología y repartición de biomasa en gramíneas nativas e introducidas de una sabana Neotropical. Ecotropicos 2 (1), 1–13.

Baruch, Z., Bilbao, B., 1999. Effects of fire and defoliation on the life history of native and invader C-4 grasses in a Neotropical savanna. Oecologia 119, 510–520.

Bilbao, B., Medina, E., 1990. Nitrogen-use efficiency for growth in a cultivated African grass and a native South American pasture grass. Journal of Biogeography 17, 421–425.

Borse, G.J., 1997. Numerical Methods with Matlab. PWS Publishing Company, Boston, MA.

Dai, A., 2010. Drought under Global Warming: A Review. Wiley Interdisciplinary Reviews: Climate Change. http://dx.doi.org/10.1002/wcc.81.

De Castro, F., Fetcher, N., 1998. Three dimensional model of the interception of light by a canopy. Agricultural and Forest Meteorology 90, 215–233.

de Moraes Frasson, R.P., Krajewski, W.F., 2010. Three dimensional digital model of a maize plant. Agricultural and Forest Meteorology 150, 478–488 (3rd ed.).

Gates, D.M., 2003. Biophysical Ecology. Dover Publications, Inc., Mineola, New York . 612 pp.

Goldstein, G., Sarmiento, G., 1987. Water relations of trees and grasses and their consequences for the structure of savanna vegetation. In: Walker, B.H. (Ed.), Tropical Savanna Determinants. IRL Press, Oxford, pp. 13–38.

Guswa, A.J., Celia, M.A., Rodriguez-Iturbe, I., 2002. Models of soil moisture dynamics in ecohydrology: a comparative study. Water Resources Research 38 (9), 5-1–5-15.

Hill, M.J., Hanan, M.P., 2010. Ecosystem Function in Savannas: Measurement and Modeling at Landscape to Global Scales. CRC Press.

Hodgkinson, K.C., Ludlow, M.M., Mott, J.J., Baruch, Z., 1989. Comparative responses of the savanna grasses *Cenchrus ciliaris* and *Themeda triandra* to defoliation. Oecologia 79, 45–52.

Laio, F., Porporato, A., Ridolfi, L., Rodríguez-Iturbe, I., 2001. Plants in water-controlled ecosystems: active role in hydrologic processes and response to water stress II. Probabilistic soil moisture dynamics. Advances in Water Resources 24, 707–723.

Larcher, W., 2003. Physiological Plant Ecology, 4th ed. Springer, Germany.
Mata, L.J., 1996. A study of climate change impacts on the forest of Venezuela. In: Smith, J., Bhatti, N., Menzhulin, G., Benioff, R., Budyko, M.I., Campos, M., Jallow, B., Rijsberman, F. (Eds.), Adapting to Climate Change: An International Perspective. Springer- Verlag, New York, NY, USA.
Monsi, M., Saeki, T., 1953. Über den Lichtfaktor in den Pflanzengesellschaften und seine Bedeutung für die Stoffproduktion. Japanese Journal of Botany 14, 22–52.
Monteith, J.L., Unsworth, M., 1973. Principles of Environmental Physics. Butterworth-Heinemann, Oxford.
Oyarzun, R.A., Stöckle, C.O., Whiting, M.D., 2007. A simple approach to modeling radiation interception by fruit-tree orchards. Agricultural and Forest Meteorology 142 (1), 12–24.
Pearcy, R.W., Yang, W., 1996. A three-dimensional crown architecture model for assessment of light capture and carbon gain by understory plants. Oecologia 108, 1–12.
Porporato, A., Laio, F., Ridolfi, L., Rodríguez-Iturbe, I., 2001. Plants in water-controlled ecosystems: active role in hydrologic processes and response to water stress III. Vegetation water stress. Advances in Water Resources 24, 725–744.
Raventós, J., Silva, J.F., 1988. Architecture, seasonal growth and interference in three grass species with different flowering phenologies in a tropical savanna. Vegetatio 75, 115–123.
Raventós, J., Segarra, J., Acevedo, M.F., 2004. Growth dynamics of tropical savanna grass species using projection matrices. Ecological Modelling 174, 85–101.
Rosati, A., Badeck, F.W., Dejong, T.M., 2001. Estimating canopy light interception and absorption using leaf mass per unit leaf area in *Solanum melongena*. Annals of Botany 88, 101–109.
Sankaran, M., Ratnam, J., Hanan, N.P., 2004. Tree–grass coexistence in savannas revisited — insights from an examination of assumptions and mechanisms invoked in existing models. Ecology Letters 7, 480–490.
Sarmiento, G., 1983. The savannas of tropical America. In: Bourlière, F. (Ed.), Tropical Savannas. Ecosystems of the World, vol 13. Elsevier Scientific Publishing Company, Amsterdam-Oxford-New York, pp. 245–285. 730 pp.
Sarmiento, G., 1984. The Ecology of Neotropical Savannas. Harvard University Press, Cambridge. Mass . 235 pp.
Segarra, J., Raventós, J., Acevedo, M.F., 2005. Growth of tropical savanna grass plants in competition: a shoot population model. Ecological Modelling 189, 270–288.
Segarra, J., Acevedo, M.F., Raventós, J., García-Núñez, C., Silva, J.F., 2009. Coupling soil water and shoot dynamics in three grass species: a spatial stochastic model on water competition in Neotropical savanna. Ecological Modelling 220, 2734–2743.
Segarra, J., Raventós, J., Acevedo, M.F., 2010. Savanagua: a spatially explicit competition modeling of savanna ecosystems. In: Veress, B., Szigethy, J. (Eds.), Horizons in Earth Science Research, volume 4. Nova Publishers.
Sekimura, T., Roose, T., Li, B., Maini, P.K., Suzuki, J., Hara, T., 2000. The effect of population density on shoot morphology of herbs in relation to light capture by leaves. Ecological Modelling 128, 51–62.
Silva, J.F., 1987. Dynamics responses of savannas to stress and disturbance: species dynamics. In: Walker, B.H. (Ed.), IUBS n. 3, Determinants of Tropical Savannas. IRL Press, Oxford, pp. 141–156.
Silva, J.F., Castro, F., 1989. Fire, growth and survivorship in a Neotropical savanna grass (*Andropogon semiberbis* in Venezuela. Journal of Tropical Ecology 5, 387–400.
Silva, J.F., Sarmiento, G., 1976. La composición de las sabanas en Barinas en relación con las unidades edáficas. Acta Científica Venezolana 27, 68–78.
Sinoquet, H., Rakocevic, M., Varlet-Grancher, 2000. Comparison of models for daily light partitioning in multispecies canopies. Agricultural and Forest Meteorology 101, 251–263.
Solbrig, O.T., 1993. Ecological constraints to savanna land use. In: Young, M.D., Solbrig, O.T. (Eds.), The World's Savannas: Economic Driving Forces Ecological Constrainte. Parthenon Press, Paris, pp. 21–48.
Staver, A.C., Archibald, S., Levin, S.A., 2011a. Tree cover in sub-Saharan Africa: rainfall and fire constrain forest and savanna as alternative stable states. Ecology 92, 1063–1072.
Staver, A.C., Archibald, S., Levin, S.A., 2011b. The global extent and determinants of savanna and forest as alternative biome states. Science 334, 230–232. http://dx.doi.org/10.1126/science.1210465.
Thornley, J.H.M., 2002. Instantaneous canopy photosynthesis: analytical expressions for sun and shade leaves based on exponential light decay down the canopy and an acclimated non-rectangular hyperbola for leaf photosynthesis. Annals of Botany 89, 451–458.
TuTiempo.com, 2011. Clima en Barinas. http://www.tutiempo.net/clima/Barinas/804400.htm Last accessed Feb 1, 2011.
Wang, S.S., Grant, R.F., Verseghy, D.L., Black, T.A., 2001. Modeling plant carbon and nitrogen dynamics of a boreal aspen forest in CLASS — the Canadian Land Surface Scheme. Ecological Modelling 142, 135–154.
Williams, D.G., Black, R.A., 1994. Drought response of a native and introduced Hawaiian grass. Oecologia 97, 512–519.